MICROSCOPY RESEARCH & TECHNIQUE

STROMAL CELLS OF GIANT CELL TUMOUR OF BONE SHOW PRIMARY CILIA

Journal:	*Microscopy Research and Technique*
Manuscript ID	MRT-21-195.R2
Wiley - Manuscript type:	Research Article
Date Submitted by the Author:	n/a
Complete List of Authors:	Castiella, Tomás; Aragon Health Sciences Institute Iruzubieta, Pablo; University of Zaragoza Faculty of Medicine, Human Anatomy and Histology Monleon, Eva; University of Zaragoza Faculty of Medicine, Human Anatomy and Histology Cardiel, Mª José; Lozano Blesa University Clinical Hospital, Pathology Gómez-Vallejo, Jesús; Lozano Blesa University Clinical Hospital, Orthopaedics Monzón, Marta; University of Zaragoza Faculty of Medicine, Human Anatomy and Histology Junquera Escribano, Concepcion; University of Zaragoza Faculty of Medicine, Human Anatomy and Histology
Classifications:	transmission electron microscopy < ELECTRON MICROSCOPY, fluorescence microscopy < LIGHT MICROSCOPY
Keywords:	Giant Cell Tumor of Bone, Ultrastructure, Primary cilia, Hh signaling pathway

STROMAL CELLS OF GIANT CELL TUMOR OF BONE SHOW PRIMARY CILIA

PRIMARY CILIA IN GIANT CELL TUMOR OF BONE

Tomás Castiella MD, PhD[1(*)], Pablo Iruzubieta MD[2(*)], Eva Monleón PhD[2], Mª José Cardiel MD[1], Jesús Gómez-Vallejo MD[3], Marta Monzón PhD[2], Mª Concepción Junquera PhD[2]

1 Department of Pathology, Hospital ClínicoUniversitario Lozano Blesa

2 Department of Human Anatomy and Histology, Faculty of Medicine, University of Zaragoza

3 Department of Traumatology and Orthopaedic Surgery, Hospital ClínicoUniversitario Lozano Blesa

(*)TC and PI are first co-authors

Institute for Health Research Aragón (IIS), Domingo Miral s/n, 50009 Zaragoza, Spain

CorrespondingAuthor: *Pablo Iruzubieta, pablo.iruzubieta@hotmail.es*

Phone: 00 34 976 761674

ORCID:

Tomás Castiella: 0000-0001-7453-2470

Pablo Iruzubieta: 0000-0003-0331-6222

Eva Monleón: 0000-0002-7453-1766

Marta Monzón: 0000-0002-2787-9671

Concepción Junquera: 0000-0002-9951-107

ABSTRACT

Giant cell tumor of bone (GCTB) is a locally aggressive primary bone neoplasm composed by tumoral stromal cells and reactive monocytic/histiocytic cells that fuse to form osteoclast-like multinucleated cells. Recently, specific histone 3.3 mutations have been demonstrated in stromal cells of GCTB. Many of the pathways related to bone proliferation and regulation depend on the primary cilium, a microtubule-based organelle which projects outside the cell and acts as a sensorial antenna. In the present work, we aimed to study the presence and role of primary cilia in GCTB.

Ultrastructural, immunohistochemical and immunofluorescence studies were performed in order to demonstrate thatthe primary cilium is located in spindle-shaped stromal cells of GCTB. Moreover, we showed Hh signalling pathway activation in these cells. Hence, primary cilia may play a relevant role in GCTBtumorigenesis through Hh signalling activation in stromal cells.

Keywords: Giant cell tumor of bone, ultrastructural study, primary cilium, Hh signalling pathway

Research highlights

- Transmission electron microscopy allows to describe and differentiate cellular subpopulations in Giant Cell Tumor of Bone.
- The primary cilium is present in some tumoral Stromal Cells of Giant Cell Tumor of Bone.
- Hedgehog signalling is activated in these cells.

1. INTRODUCTION

According to the World Health Organisation (WHO) definition, giant cell tumor of bone (GCTB) is a locally aggressive primary bone neoplasm composed of proliferative mononuclear stromal cells (SCs), numerous reactive macrophages and large osteoclast-like multinucleated giant cells (GCs) (Athanasou et al., 2013). GCTB usually appears in young adults' metaphysis-epiphysis of long tubular bones. Although malignant transformation in GCTB is uncommon, pulmonary metastasis have been occasionally described (Athanasou et al., 2013).

Two mixed mononuclear cell types are present in the GCTB: monocyte-macrophage CD14+/CD68+ cells and SCs (Wülling et al., 2003). Nowadays, it is accepted that SCs represent the proliferative tumoral component of the GCTB; meanwhile, reactive multinucleated GCs are originated from blood monocytes recruited into the tumoral tissue (Wülling et al., 2003; Kim et al., 2012;). Recently, the mutation G34W in Histone H3 has been proved as a useful diagnostic marker of SC in GCTB (Cleven et al., 2015).

Previous ultrastructural studies dealing with GCTB have been focused on characterization of mononuclear cells and their osteoblastic or osteoclastic differentiation (Anazawa et al., 2006; Aparisi et al., 1977; Garcia et al., 2013). Furthermore, ultrastructural similarities between GCTB giant cells with physiological osteoclasts and with multinucleated GCs in lesions that mimic GCTB have been also reported (Anazawa et al., 2006).

The primary cilium is a microtubular non-motile structure composed of a 9+0 axoneme originated from a modified centriole which projects to the extracellular medium (Malicki & Johnson, 2017). Its presence in skeletal cells was detected almost 50 years ago (Tonna & Lampen, 1972). The potential role that this organelle may play in bone development and homeostasis was proposed in the early 21st century(Whitfield, 2003). However, there is increasing evidence that primary cilia-dependent signalling

pathways, like Hedgehog (Hh) ~~and Wnt~~, play a crucial role in regulating mammalian bone development and turnover (Day & Yang, 2008). Thus, Hh pathway activation is necessary for Runx2 expression, a transcription factor essential for correct osteoblast differentiation (Rutkovskiy et al., 2016).

Three Hh ligands have been described: Sonic (Shh), Indian (Ihh) and Desert (Dhh) (Ramsbottom & Pownall, 2016). Ihh has been mainly involved in bone formation (Yang et al., 2015). When these ligands bind the transmembrane receptor Patched (located in the ciliary membrane) it is removed from primary cilia, allowing Smo entrance in ciliary axoneme. Then, Gli proteins are activated and translocated into the cellular nucleus, where they promote target gene transcription (including Runx2) (Chahal et al., 2018). Hh activation enhances expression of genes related to proliferation, angiogenesis or epithelial-mesenchymal transition (Chahal et al., 2018). Thus, excessive Hh signalling activation leads tumor formation and maintenance of cancer stem cells (Chahal et al., 2018). Moreover, ciliary proteins, including Arl13b, have been shown to be essential in Hh signalling and in its oncogenic implications (Larkins et al., 2011; Bay et al., 2018).

Here, we show for the first time that SCs of GCTB present primary cilia. This finding might have important implications in these tumors through Hh signalling pathway activation.

2. METHODS

Six GCTB samples biopsied from patients were included in the present study. All samples were provided by the *Hospital Clínico Lozano Blesa*from Zaragoza. All the protocols developed were approved by the Human Research Ethics Committee of Aragon (CEICA) and were in accordance with Helsinki Declaration.

2.1. Electron Microscopy

A piece of every tumorconsisting of 2.5x2.5mmwas immersed in 2.5% glutaraldehyde for fixation for 4-6h. The samples were washed in PB, post-fixed with 2% osmium, rinsed, dehydrated in graded ethanol, stained with 2% uranyl-acetate, cleared in propylene oxide and embedded in araldite (Durcupan, Fluka). Serial semi-thin sections (1.5µm) were cut and lightly stained with 1% toluidine blue. Later, ultrathin (0.08µm) sections were cut with a diamond knife, collected on Formvar coated single-slot grids, counter-stained with 1% uranyl acetate and Reynold's lead citrate for 10minutes. They were examined by a JEOL-JEM-1010 transmission electron microscope (TEM). The images were captured with GatanBioscan Camera with pixel size 6.45µm x 6.45µm and spatial resolution of 1024,1024, 1, 1 (x, y, z, t) and automatic gain (assigning a brightness value to each pixel depending on the clearest and the darkest intensity in every image and highlighting electrondensity contrast).

2.2. Immunohistochemistry

Samples were processed according to standard histological procedures and stained with hematoxylin and eosin (H&E). Immunohistochemical staining was performed on formalin-fixed paraffin-embedded 4-µm thicksections. All immunohistochemical products except primary antibody were obtained from DAKO (Denmark). Primary antibodies used in this study were: monoclonal rabbit anti-Histone H3.3 G34W (2.5 µg/mL, Quimigen S.L., 31-1145-00, Madrid, Spain), polyclonal rabbit anti-Gli1 (1:200, ABCAM, ab49314, Cambridge, UK), polyclonal rabbit anti-Smo (1:1000, LS Bioscience, LS-B4911, Seattle, USA) and polyclonal goat anti-Patched (1:100, Santa Cruz, sc-6149, Dallas, USA). Tissue sections were deparaffinised and hydrated using routine methods and then subjected to heat-induced antigen retrieval. For Gli1 and Smo, buffer citrate pH6 was used and the samples were treated during 6 minutes in an 800-W microwave and at 360 W for 5 additional minutes. For H3.3 G34W and Patched staining, samples were treated at 96ºC for 20 min in EnVision™ FLEX Target Retrieval

solution High pH. Endogenous peroxidase was blocked for 30 minutes and sections were washed in distilled water and PBS 3 min, twice.

Afterwards, sections were incubated with primary antibodies at 4°C overnight in a humidified chamber, washed in PBS three times and incubated with secondary antibody Rabbit-Mouse Labelled Polymer-Dako EnVision-HRP or Polyclonal Rabbit Anti-Goat Immunoglobulins/HRP (1:200) for 1 hour. 3,3'diaminobenzidine was used as chromogen. The samples were washed twice in distilled water, contrasted with Mayer's hematoxylin for 7 min, washed in tap water for 15 min, dehydrated in a graded series of ethanol, cleared in xylene and cover slipped with Eukitt.

Negative controls where based on samples were no primary antibody was added. All antibodies were commercial and supposedly validated.

All samples were analysed and digital images from representative areas were captured by Olympus BX53 and Olympus UIS UPLFLN Series objectives. FN: 26.5. 20x AN 0.5 and 40x AN 0.75. Images were captured with Olympus DP72 Digital Camera. Pixel size 6.45µm x 6.45µm, total number of pixel 1.5 million. Exposition mode: SFL Auto and spatial resolution of 4140x3096x1x1 (x, y, z, t).

2.3. Double Immunofluorescence Microscopy

Formalin-fixed paraffin-embedded tissues were deparaffinised and hydrated. Then, antigen retrieval was performed at 96ºC for 20 min in EnVision™ FLEX Target Retrieval solution High pH. Sections were incubated overnight at 4°C with the following antibodies: mouse-monoclonal anti-Acetylated tubulin (1:4000, Sigma Aldrich, T7451; St. Louis, MO, USA), mouse monoclonal anti-Arl13b (1:50, Proteintech, 66739-1-Ig, Manchester, UK)and rabbit-monoclonal anti-Histone H3.3 G34W (2.5 µg/mL, Quimigen S.L., 31-1145-00, Madrid, Spain). They were washed in PBS and incubated with the respective secondary antibodies: anti-Mouse AlexaFluor594 (1:1000, ThermoFisher R37115; Waltham, MA, USA) and anti-Rabbit AlexaFluor488 (1:1000, ThermoFisher A-

21206; Waltham, MA, USA) for 1 hour at RT. Incubations were performed in a dark humidified chamber. After washing in PBS, DAPI (1 µg/mL, Sigma-Aldrich) was added for 1 minute for nuclei counterstaining. Sections were washed in PBS and covered with DAKO Fluorescence mounting medium.

All antibodies were commercial and supposedly validated.

Images were analysed using the following filters: U-MNUA2 for DAPI, U-MWIABA2 for Alexa Fluor 488 and U-MWIG2 for Alexa Fluor 594 in a Olympus BX53 microscope and Olympus UIS UPLFLN Series objectives. FN: 26.5. 20x AN 0.5 and 40x AN 0.75. Images were captured with Olympus DP72 Digital Camera. Pixel size 6.45µm x 6.45µm, total number of pixel 1.5 million. Exposition mode: Auto and spatial resolution of 4080x3072x1x1 (x, y, z, t). Images were analysed with DP Controller Software. Every fluorescent channel was individually photographed and channels were merged using FIJI Image_J software, where contrast and brightness were adjusted (Schindelin et al., 2012).

Statistical analyses were performed counting ciliated cells per High Power Field (HPF = x400) and using a non parametric test (Mann-Whitney U).Hence, representative areas were analysed (total of 18 images). In each HPF, between 70 and 100 mononuclear cells were present while the number of giant cells ranges from 0 to 7.

3. RESULTS

3.1. Preliminary histological study.

Histopathological techniques routinely confirmed the diagnosis of GCTB (Fig.1). Thus, H&E revealed the presence of multinuclear GCs scattered among mononuclear cells (Fig.1a). CD68 antibody labelled mononuclear histiocytic cells and multinucleated GCs (Fig.1b) while Histone H3.3 mutation G34W antibody labelled tumoral SCs (Fig.1c). Ki67was exclusively expressed by mononuclear cells(Fig.1d).

3.2. GCTB ultrastructural findings

Electron microscopy examination evidenced two well-defined groups: mononuclear and multinucleated giant cells. In turn, mononuclear cells included two different phenotypes based on cytoplasm electrondensity and nuclear chromatin condensation. Thus, histiocytic cells showed lesser electrondensity and homogenous chromatin, while SCs cytoplasm were more electrondense and their nuclei showed condensed chromatin constituting marginal clusters in contact with nuclear envelope (Fig.2a).

SC morphology varied from fusiform-spindle to oval. They showed fine membrane prolongations contacting neighbour cells (Fig.2b). They presented cytoplasmic electron-light no-membranous inclusions conferring a characteristic vacuolated appearance (Fig.2b). Some mitochondria, scarce granular endoplasmic reticulum and abundant free ribosomes were observed. Centrioles, located near nuclei, showed subdistal appendages and they were related to intermediate filaments and numerous Golgi-derived vesicles (Fig.2c-d). All these findings are suggestive ofcentriolar activation.

Primary cilia were specifically observed in SCs (Fig.2e-f). Primary ciliogenesisis sequentially ordered in Figure 3. Firstly, the ciliary vesicle (constituted by fusion of Golgi-derived vesicles) localizes on the distal pole of the mother centriole, which forms cilia basal body (Fig.3a). Then, the 9+0 axoneme grew from the basal body (Fig. 3b). Occasionally, abnormal duplication of centrioles was evidenced by detection of three centrioles, two of them originating cilia (Fig.3c). Figures 3d and 3e show ultrastructural features corresponding to a primary cilium in its maximum length. Basal body presented subdistal appendages and was anchored to cell membrane by transition fibres. The axoneme was originated from the basal body and it was located in a cell membrane invagination called ciliary pocket, where coated vesicles are concentrated as a sign of important molecular exchange (Fig.3e). In some ciliated cells, nuclei showed characteristic nuclear envelope prolongations (Fig. 3d-e). These nuclear structures have been previously called envelope-limited chromatin sheets (ELCS).

Primary ciliain these cells are originated from no-displaced centrioles and, therefore, goes through the cytoplasm towards the extracellular medium.

The mononuclear histiocytic cells showed a less electrondense cytoplasm (Fig.4a), with abundant mitochondria, granular endoplasmic reticulum and prominent Golgi apparatus. Although their nuclei showed a diverse morphology, peripheral nucleoli were always found. They presented many lysosomes and fine phagocytic prolongations (Fig.4b). These cells contact each other through cytoplasmic prolongations (Fig.4b). A reduced number of these histiocytic cells showed scarce organelles, abundant ribosomes and multivesicular bodies, all features suggestive of an undifferentiated phenotype (Fig. 4c).

Multinucleated GCs included 10 to 30 nuclei. They showed oval or irregular morphology and an electron light appearance. They presented a fine marginal chromatin contacting nuclear membrane and prominent nucleoli (Fig.4d). Their cytoplasm presented a homogenous distribution of organelles, abundant mitochondria and lipid inclusions (Fig. 4d). Surrounding multinucleated GCs, both, mononuclear histiocytic and stromal cells were located. Although defining dynamic processes from TEM is always difficult, we could observe light undifferentiated histiocytic cells merging with GCs and syncytial membrane disappearance, suggestive of cellular fusion (Fig.4e).

Some reactive foam cells plenty of electron lucent vacuoles were also found in these tumors. They were probably involved in phagocytic processes as they showed lysosomes with different content (Fig.4f). Few disperse lymphocytes and granulocytes were also observed, the latter being involved in macropinocytosis processes.

3.3. Primary cilia and Hh signalling presence in GCTB

Immunofluorescent co-localisation of Histone H3.3 mutation G34W (specific for SCs of GCTB) and Acetylated-tubulin (marker for cilia axoneme) and Arl13b (marker for ciliary

membrane) showed that stromal cells presented primary cilia (Fig. 5, Suppl. Fig. 1). Primary cilia were usually located near nuclei, in agreement with electron microscopy findings. Quantitative analyses showed that around 7 mononuclear cells per High Power Field (x400) were ciliated, which supposed around 10% of mononuclear cells, while no multinucleated giant cell presented cilia (Suppl. Fig.2).

Furthermore, the implications of primary cilia in GCTB were studied by analysis of the activation of Hh signalling pathway, a well-known cilia-dependent pathway related to tumorogenesis and bone regulation. Immunohistochemical experiments for Hh pathway protein Patched, Smo and Gli1 were performed (Suppl. Fig. 3, Fig. 6). Patched (Suppl. Fig. 3a) and Smo (Suppl. Fig. 3b) staining were located in paranuclear regions while Gli1 labelled subtly but clearly cells nuclei (Fig. 6a-c). Nuclear staining of Gli1 is a sign of Hh signalling activation. Thus, these results suggest that Hh signalling pathway is present and activated in SCs of GCTB.

4. DISCUSSION

The nature and cellular components of GCTB have constituted the subject of multiple previous studies. Most of them wrongly identified all mononuclear cells as stromal cells based on conventional microscopy morphology. However, histochemical and electron microscopy techniques shed light on cells identification (Hanaoka et al., 1970; Aparisi et al., 1977).In this study we have accurately defined ultrastructural features of the two different mononuclear cell populations identified by cytoplasm electrondensity and nuclear chromatin condensation. Cells showing lesser electrodensity and homogenous chromatin are called histiocytic cells here. The round histiocytic cells previously described by other authors may correspond to activated histiocytes with phagocytic capacity (Hanaoka et al., 1970; Aparisi et al., 1977). Intermediate phenotypes are compatible with resting, activated or prior to giant cell formation stages.

The second mononuclear cell type, stromal cells (SCs), show higher electrondensity in their cytoplasm and nuclei with condensed chromatin forming marginal clusters in

contact with nuclear envelope. This phenotype corresponds to stromal cells type 1 of Aparisi (Aparisi et al., 1977). However, phenotypic variability appears. Probably, those presenting features suggestive of undifferentiation may suppose cancer stem cells. SCs have been defined as immature fibroblasts or primitive osteoblasts. Their close histogenic relationship with osteoblasts is based on focal deposition of osteoid seen in one third of GCTB (Spjut et al., 1983). Additionally, bone tissue is not only produced by reactive osteoblasts but also by SCs (Goldring et al., 1987). According with the results provided here, SCs are clearly defined as mesenchymal cells presenting special and exclusive ultrastructural features such as presence of large electron-light vacuoles, peculiar density of cytoplasm and activation of centrioles. The most novel finding provided in the present study is the presence of primary cilia in these cells.

Primary cilia in osteoblasts and osteocytes contributes to bone formation and homeostasis(Mitchison & Valente, 2017). Furthermore, the participation of primary cilia in different types of cancer of epithelial and mesenchymal line has been demonstrated. Nevertheless, the prevalence of cilia on human tumors remains unclear, and their role in cancer is just beginning to be explored (Eguether & Hahne, 2018; Fabbri et al., 2019). In human osteosarcoma MG63 cell line the number of ciliated cell is significantly higher than expected (Kowal & Falk, 2015).

The cilia-dependant Hh signalling pathway plays a key role in both bone physiology and pathology. Thus, it is essential for temporal and spatial regulation of bone remodelling (Rodda, 2006; Yang et al., 2015). Moreover, Hh signalling pathway (especially through the Ihh ligand) stimulates intramembranous and endochondral ossification, bone turnover and remodelling of fractures sites (Yang et al., 2015).

The deregulation of Hh signalling pathway has been linked to some skeletal development diseases (Rodda, 2006; Yang et al., 2015) and tumors (Scales & de Sauvage, 2009). Furthermore, Hh signalling pathway in osteosarcoma was related to radio-resistance and invasiveness (Qu et al., 2018). Interestingly, the ciliary membrane

protein Arl13b plays an essential role in tumoral Hh signalling through primary cilia (Bay et al., 2018).

Here, we show Hh pathway activation in some SCs. These results are in accordance with Horvai et al. (2012) where 10% of mononucleated cells expressed Ihh (we found a similar proportion of ciliated cells, as it is described above). Besides, Horvai et al. also showed that GCTB stromal cells expressed Runx2 (Horvai et al., 2012), a well-known downstream target of Hh signalling pathway (Rutkovskiy et al., 2016).

The observation of primary cilia and Hh pathway activation in SCs suggests their role in cellular signalling and tumorogenesis. Moreover, some ciliated SCs showed envelope-limited chromatin sheets (ELCS), a structure described in cancer and stem cells (Olins & Olins, 2009; Cebrián-Silla et al., 2017). These findings suggest that primary cilia may play an important role in quiescent cancer stem cells of GCTB. This feature would explain why only a specific population of stromal cells show primary cilia and Hh activation and they are not constitutively present in every stromal cell. Moreover, the dynamic nature of cilia assembly and Hh signalling must be taken into account while the techniques performed in this paper are mainly static.

In conclusion, our study reveals that SCs of GCTB present primary cilia. Moreover, we proved that Hh signalling pathway is activated in these cells, showing that primary cilia may play an important role in GCTB tumorogenesis and could be consequently used as a potential therapeutic target.

5. DECLARATIONS

Funding. No funding was specifically received for the experiments showed in this paper.

Competing interests. The authors declare that they have no conflict of interest.

Ethics approval and consent declarations. All protocols and consents developed were approved by the Human Research Ethics Committee "*Comité Ético de Investigación Clínica de Aragón*".

Authors contribution. TC conceived the study, performed ultrastructural experiments and contributed to write the manuscript, PI performed immunohistochemical and immunofluorescence studies and contributed to write the manuscript, EM performed immunohistochemical experiments. MJC and JGV provided the samples. MM contributed to write the manuscript. CJ conceived and supervised the study, performed ultrastructural experiments, analysed the results and contributed to write the manuscript.

Acknowledgements: Authors would like to acknowledge the use of *Servicio General de Apoyo a la Investigación*- SAI, *Universidad de Zaragoza*.

6. REFERENCES

Anazawa, U., Hanaoka, H., Shiraishi, T., Morioka, H., Morii, T., & Toyama, Y. (2006). Similarities between giant cell tumor of bone, giant cell tumor of tendon sheath, and pigmented villonodular synovitis concerning ultrastructural cytochemical features of multinucleated giant cells and mononuclear stromal cells. *Ultrastructural Pathology*, *30*(3), 151–158. https://doi.org/10.1080/01913120600689707

Aparisi, T., Arborgh, B., & Ericsson, J. L. (1977). Giant cell tumor of bone: detailed fine structural analysis of different cell components. *Virchows Archiv. A, Pathological Anatomy and Histology*, *376*(4), 273–298. http://www.ncbi.nlm.nih.gov/pubmed/145722

Athanasou, N., Bansal, M., Forsyth, R., Reid, R., & Z, S. (2013). Giant Cell Tumour of Bone. In C. Fletcher, J. Bridge, P. Hogendoorn, & F. Mertens (Eds.), *WHO Classification of Tumours of Soft Tissue and Bone* (pp. 321–324). IARC.

Bay, S. N., Long, A. B., & Caspary, T. (2018). Disruption of the ciliary GTPase Arl13b suppresses Sonic hedgehog overactivation and inhibits medulloblastoma formation. *Proceedings of the National Academy of Sciences of the United States of America*, *115*(7), 1570–1575. https://doi.org/10.1073/pnas.1706977115

Cebrián-Silla, A., Alfaro-Cervelló, C., Herranz-Pérez, V., Kaneko, N., Park, D. H., Sawamoto, K., Alvarez-Buylla, A., Lim, D. A., & García-Verdugo, J. M. (2017). Unique Organization of the Nuclear Envelope in the Post-natal Quiescent Neural Stem Cells. *Stem Cell Reports*, *9*(1), 203–216. https://doi.org/10.1016/j.stemcr.2017.05.024

Chahal, K. K., Parle, M., & Abagyan, R. (2018). Hedgehog pathway and smoothened inhibitors in cancer therapies. *Anti-Cancer Drugs*, *29*(5), 387–401. https://doi.org/10.1097/CAD.0000000000000609

Cleven, A. H. G., Höcker, S., Briaire-De Bruijn, I., Szuhai, K., Cleton-Jansen, A. M., & Bovée, J. V. M. G. (2015). Mutation analysis of H3F3A and H3F3B as a diagnostic tool for giant cell tumor of bone and chondroblastoma. *American Journal of Surgical Pathology*, *39*(11), 1576–1583. https://doi.org/10.1097/PAS.0000000000000512

Day, T. F., & Yang, Y. (2008). Wnt and hedgehog signaling pathways in bone

development. *Journal of Bone and Joint Surgery - Series A*, *90*(SUPPL. 1), 19–24. https://doi.org/10.2106/JBJS.G.01174

Eguether, T., & Hahne, M. (2018). Mixed signals from the cell's antennae: primary cilia in cancer. *EMBO Reports*, *19*(11), e46589. https://doi.org/10.15252/embr.201846589

Fabbri, L., Bost, F., & Mazure, N. (2019). Primary Cilium in Cancer Hallmarks. *International Journal of Molecular Sciences*, *20*(6), 1336. https://doi.org/10.3390/ijms20061336

Garcia, R. A., Platica, C. D., Alba Greco, M., & Steiner, G. C. (2013). Myofibroblastic differentiation of stromal cells in giant cell tumor of bone: An immunohistochemical and ultrastructural study. *Ultrastructural Pathology*, *37*(3), 183–190. https://doi.org/10.3109/01913123.2012.756092

Goldring, S. R., Roelke, M. S., Petrison, K. K., & Bhan, A. K. (1987). Human giant cell tumors of bone. Identification and characterization of cell types. *Journal of Clinical Investigation*, *79*(2), 483–491. https://doi.org/10.1172/JCI112838

Hanaoka, H., Friedman, B., & Mack, R. P. (1970). Ultrastructure and histogenesis of giant-cell tumor of bone. *Cancer*, *25*(6), 1408–1423. https://doi.org/10.1002/1097-0142(197006)25:6<1408::aid-cncr2820250622>3.0.co;2-#

Horvai, A. E., Roy, R., Borys, D., & O'Donnell, R. J. (2012). Regulators of skeletal development: A cluster analysis of 206 bone tumors reveals diagnostically useful markers. *Modern Pathology*, *25*(11), 1452–1461. https://doi.org/10.1038/modpathol.2012.110

Kim, Y., Nizami, S., Goto, H., & Lee, F. Y. (2012). Modern interpretation of giant cell tumor of bone: Predominantly osteoclastogenic stromal tumor. *Clinics in Orthopedic Surgery*, *4*(2), 107–116. https://doi.org/10.4055/cios.2012.4.2.107

Kowal, T. J., & Falk, M. M. (2015). Primary cilia found on HeLa and other cancer cells. *Cell Biology International*, *39*(11), 1341–1347. https://doi.org/10.1002/cbin.10500

Larkins, C. E., Gonzalez Aviles, G. D., East, M. P., Kahn, R. A., & Caspary, T. (2011). Arl13b regulates ciliogenesis and the dynamic localization of Shh signaling proteins. *Molecular Biology of the Cell*, *22*(23), 4694–4703. https://doi.org/10.1091/mbc.E10-12-0994

Malicki, J. J., & Johnson, C. A. (2017). The Cilium: Cellular Antenna and Central Processing Unit. *Trends in Cell Biology*, *27*(2), 126–140. https://doi.org/10.1016/j.tcb.2016.08.002

Mitchison, H. M., & Valente, E. M. (2017). Motile and non-motile cilia in human pathology: from function to phenotypes. *Journal of Pathology*, *241*(2), 294–309. https://doi.org/10.1002/path.4843

Olins, D. E., & Olins, A. L. (2009). Nuclear envelope-limited chromatin sheets (ELCS) and heterochromatin higher order structure. *Chromosoma*, *118*(5), 537–548. https://doi.org/10.1007/s00412-009-0219-3

Qu, W., Li, D., Wang, Y., Wu, Q., & Hao, D. (2018). Activation of Sonic Hedgehog Signaling Is Associated with Human Osteosarcoma Cells Radioresistance Characterized by Increased Proliferation, Migration, and Invasion. *Medical Science Monitor*, *24*, 3764–3771. https://doi.org/10.12659/MSM.908278

Ramsbottom, S., & Pownall, M. (2016). Regulation of Hedgehog Signalling Inside and Outside the Cell. *Journal of Developmental Biology*, *4*(3), 23. https://doi.org/10.3390/jdb4030023

Rodda, S. J. (2006). Distinct roles for Hedgehog and canonical Wnt signaling in specification, differentiation and maintenance of osteoblast progenitors. *Development*, *133*(16), 3231–3244. https://doi.org/10.1242/dev.02480

Rutkovskiy, A., Stensløkken, K.-O., & Vaage, I. J. (2016). Osteoblast Differentiation at a Glance. *Medical Science Monitor Basic Research*, *22*, 95–106. https://doi.org/10.12659/MSMBR.901142

Scales, S. J., & de Sauvage, F. J. (2009). Mechanisms of Hedgehog pathway activation in cancer and implications for therapy. *Trends in Pharmacological*

Sciences, *30*(6), 303–312. https://doi.org/10.1016/j.tips.2009.03.007
Schindelin, J., Arganda-Carreras, I., Frise, E., Kaynig, V., Longair, M., Pietzsch, T., Preibisch, S., Rueden, C., Saalfeld, S., Schmid, B., Tinevez, J., White, D. J., Hartenstein, V., Eliceiri, K., Tomancak, P., & Cardona, A. (2012). Fiji: an open-source platform for biological-image analysis. *Nature Methods*, *9*(7), 676–682. https://doi.org/10.1038/nmeth.2019
Spjut, H., Dorfman, H. D., Robert E., F., & Lauren V., A. (1983). *Atlas of tumor pathology. Tumors of bone and cartilage.* (1983), Armed Forces Institute of Pathology.
Tonna, E. A., & Lampen, N. M. (1972). Electron microscopy of aging skeletal cells. I. Centrioles and solitary cilia. *Journal of Gerontology*, *27*(3), 316–324. http://www.ncbi.nlm.nih.gov/pubmed/5046597
Whitfield, J. F. (2003). Primary cilium - Is it an osteocyte's strain-sensing flowmeter? *Journal of Cellular Biochemistry*, *89*(2), 233–237. https://doi.org/10.1002/jcb.10509
Wülling, M., Delling, G., & Kaiser, E. (2003). The Origin of the Neoplastic Stromal Cell in Giant Cell Tumor of Bone. *Human Pathology*, *34*(10), 983–993. https://doi.org/10.1053/S0046-8177(03)00413-1
Yang, J., Andre, P., Ye, L., & Yang, Y. Z. (2015). The Hedgehog signalling pathway in bone formation. *International Journal of Oral Science*, *7*(2), 73–79. https://doi.org/10.1038/ijos.2015.14

FIGURE LEGENDS

Fig. 1. Histological diagnosis and preliminary study of GCTB. a) Hematoxylin-Eosin staining shows two cellular types in GCTB: mononuclear and multinuclear giant cells (GC). Some of the mononuclear cells showed a characteristic paranuclear vacuole (arrow).Scale bar = 50μm b) CD68 is a specific marker for monocyte-macrophage lineage. Thus, histiocytic mononuclear cells and giant cells (GC) expressed CD68.Scale bar = 50μm c) Histone H3.3 G34W mutation is a specific marker of the stromal neoplastic cells of GCTB. According to this, only mononuclear cells were stained, some of them expressing paranuclear vacuoles (arrow).Scale bar = 50μm d) Immunolabeling for Ki67, marker of cell cycle activation and proliferation, stained uniquely mononuclear cells. Scale bar = 100μm

Fig.2. TEM examination. Ultrastructural features of mononuclear cells of GCTB. a) Histiocytic (* light) and stromal (dark) cells are the main mononuclear components of GCTB. Scale bar = 5μmb) Stromal cells (SCs) show large paranuclear vacuoles

(v).Scale bar = 2μm c-d) Centriole activation at different stages. Note the numerous small vesicles (vs), subdistal appendages (s) and intermediate filaments (if) in relation with centrioles; features related to centriolar activation. Scale bar = 500nm e) Primary cilia in a SC. Scale bar = 2μm f) Magnification of squared area in e.Scale bar = 500nm. ax: axoneme, bb: basal body,v: vacuoles, vs: vesicles, if: intermediate filaments, mt: microtubule, s: subdistal appendages, g: Golgi

Fig.3. TEM examination. Primary cilia in stromal cells of GCTB. a) At the beginning of ciliogenesis, small vesicles derived from Golgi-apparatus fuse in a ciliary vesicle (cv) which localizes on top of the basal body (bb).Scale bar = 500nm b) Axoneme (ax) originates from basal body and is surrounded by a cell membrane invagination called ciliary pocket (cp). Daughter centriole shows pericentriolar satellites (s). Scale bar = 500nm c) Tumoral cells exceptionally showed centriole duplication, with two cilia emerging. Scale bar = 500nm d) SC shows envelope-limited chromatin sheet (elcs) and primary cilium.Scale bar = 1μm e) Primary cilium ultrastructural features. Scale bar = 1μm. mt: microtubule, if: intermediate filaments, pr: polyribosomes, vs: vesicles, sa: subdistal appendages, s: satellites, arrow: ciliary pocket, black arrowhead: transition fibres, white arrowhead: coated vesicles, bb: basal body, ax: axoneme.

Fig.4. TEM examination. Ultrastructural features of reactive cells: histiocytic light cells and multinucleated giant cells. a) Histiocytic cells show less electrondense cytoplasm than SCs and prominent nucleoli (ni). Scale bar = 2μm b) Organelle distribution of histiocytic cells. Ly: lysosomes. Encircled: intercellular contact.Scale bar = 1μm c) Detailed area of histiocytic cells organelles showing mitochondria (mt) surrounded by endoplasmic reticula (er) near a multivesicular body (mvb).Scale bar = 500nm d) Giant Cells show multiple nuclei with prominent nucleoli (ni). Moreover, its cell membrane shows short prolongations. A stromal cell (SC) appears near the GC. Scale bar = 5μm e) A histiocytic cell seems to fuse with GC (arrows point cell

membrane disappearance). Scale bar = 5μm f) Foam cells sometimes show lysosomes (ly) containing inclusions of different source.Scale bar = 5μm

Fig.5.Stromal cells show primary cilia. a) Immunofluorescent co-localisation of Histone H3.3 G34W mutation in green and Arl13b (ciliary membrane) in red showed that some stromal cells present primary cilia. Scale bar = 20μm b-d) Magnification of cells showing Histone H3.3 G34W mutation and Arl13b co-localisation.

Fig. 6. Immunohistochemical study of Hh pathway activation. a-c) Nuclear labeling of Gli1 was present in some mononuclear cells, showing activation of Hhsignaling pathway. GC: Giant Cell.Scale bar = 20μm

SupplementaryFig. 1. Immunofluorescence study of primary cilia in SCs GCTB. Co-localisation of Acetylated tubulin (red) and H3.3 G34W (green) give supporting evidence of cilia in SCs of GCTB.Scale bar = 50μm

Supplementary Fig. 2. Quantitative analysis of primary cilia presence in GCTB cells. Number of cells showing primary cilia per High-Power Field (HPF: x400). 18 representative images were analysed in total. In each HPF, between 70 and 100 mononuclear cells were present while the number of giant cells ranges from 0 to 7. No multinucleated giant cells showed primary cilia, while around 7 to 8 mononucleated cells (mean of 7,53) per HPF were ciliated (approximately 10% of total mononucleated cells). Results are expressed as mean ± SEM. Mann-Whitney U Test showed a statistical significance ($p<0,00001$).

Supplementary Fig. 3. Smo and Patched staining in GCTB. a) Some mononuclear cells showed paranuclear staining for Patched. Scale bar = 20μm b) Similarly, only mononuclear cells showed paranuclear expression of Smo. Scale bar = 20μm.

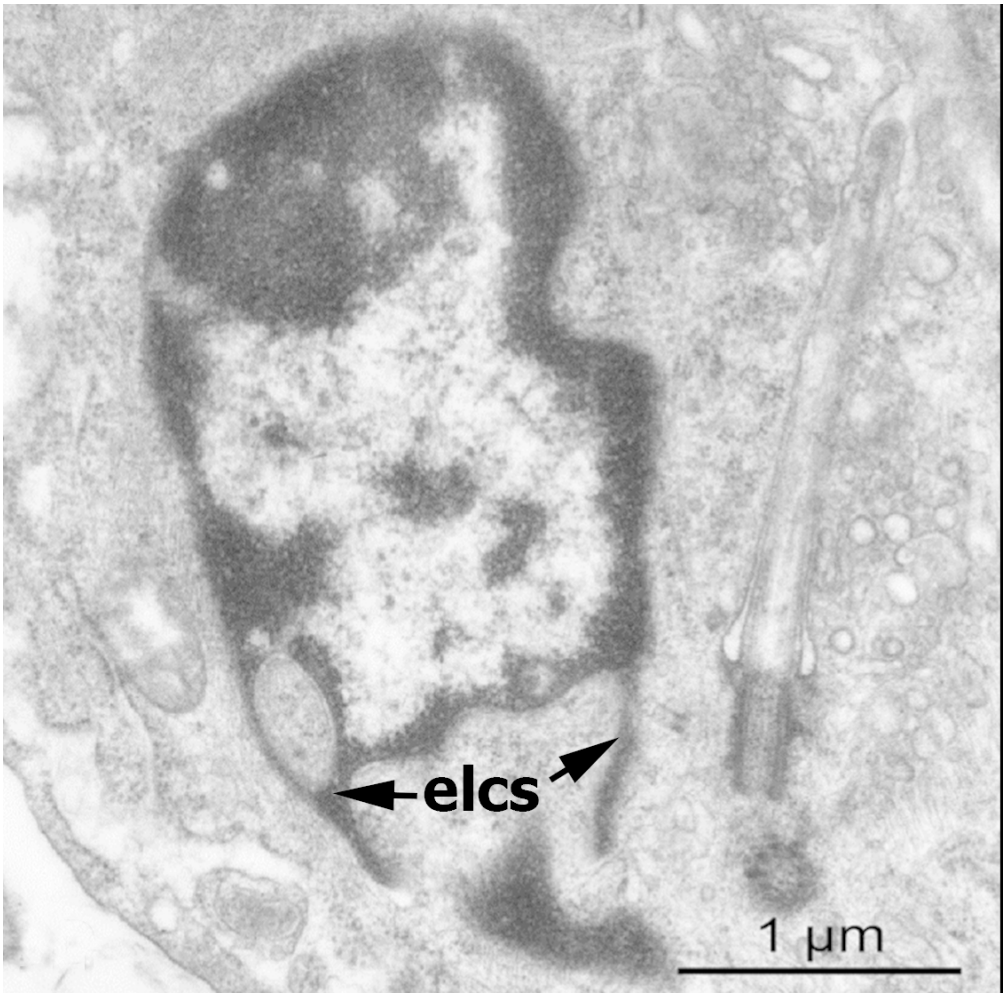
elcs
1 µm

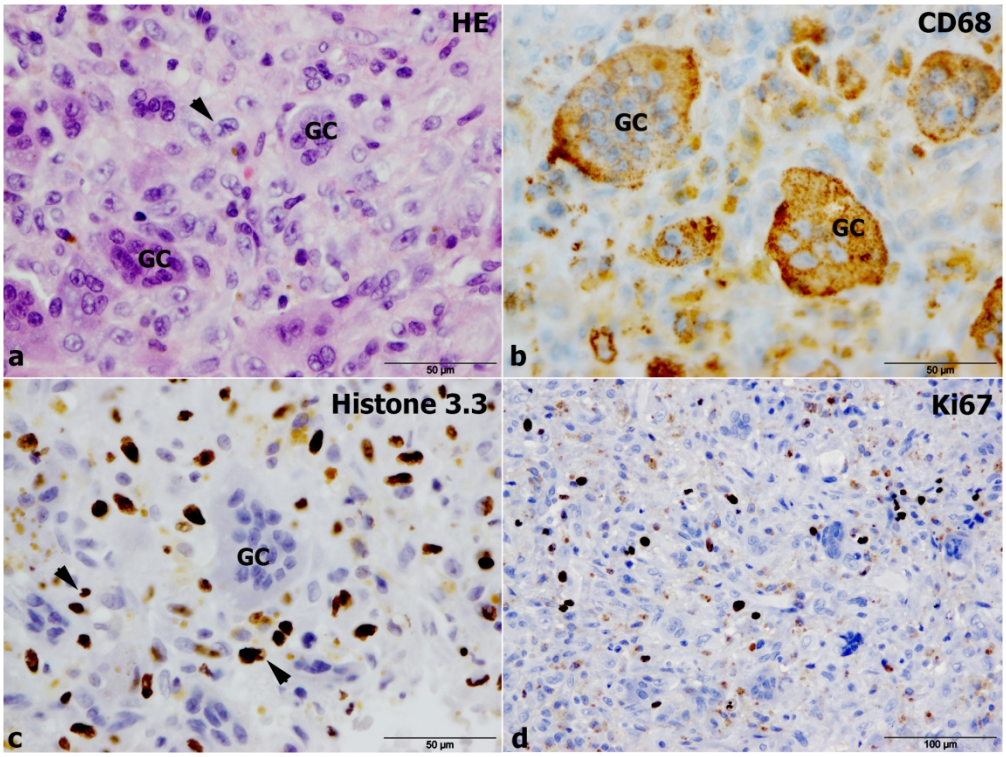

Fig. 1. Histological diagnosis and preliminary study of GCTB. a) Hematoxylin-Eosin staining shows two cellular types in GCTB: mononuclear and multinuclear giant cells (GC). Some of the mononuclear cells showed a characteristic paranuclear vacuole (arrow). Scale bar = 50µm b) CD68 is a specific marker for monocyte-macrophage lineage. Thus, histiocytic mononuclear cells and giant cells (GC) expressed CD68. Scale bar = 50µm c) Histone H3.3 G34W mutation is a specific marker of the stromal neoplastic cells of GCTB. According to this, only mononuclear cells were stained, some of them expressing paranuclear vacuoles (arrow).Scale bar = 50µm d) Immunolabeling for Ki67, marker of cell cycle activation and proliferation, stained uniquely mononuclear cells. Scale bar = 100µm

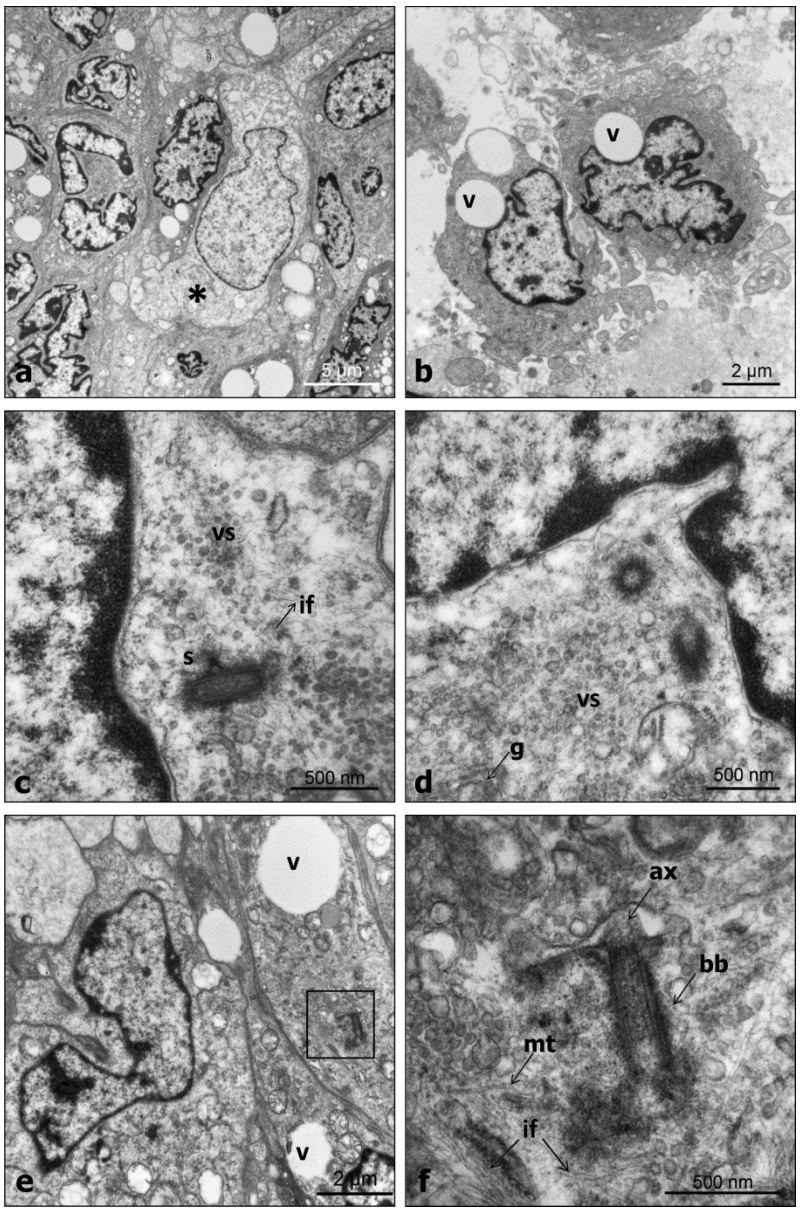

Fig.2. TEM examination. Ultrastructural features of mononuclear cells of GCTB. a) Histiocytic (* light) and stromal (dark) cells are the main mononuclear components of GCTB. Scale bar = 5µm b) Stromal cells (SCs) show large paranuclear vacuoles (v). Scale bar = 2µm c-d) Centriole activation at different stages. Note the numerous small vesicles (vs), subdistal appendages (s) and intermediate filaments (if) in relation with centrioles; features related to centriolar activation. Scale bar = 500nm e) Primary cilia in a SC. Scale bar = 2µm f) Magnification of squared area in e. Scale bar = 500nm. ax: axoneme, bb: basal body, v: vacuoles, vs: vesicles, if: intermediate filaments, mt: microtubule, s: subdistal appendages, g: Golgi

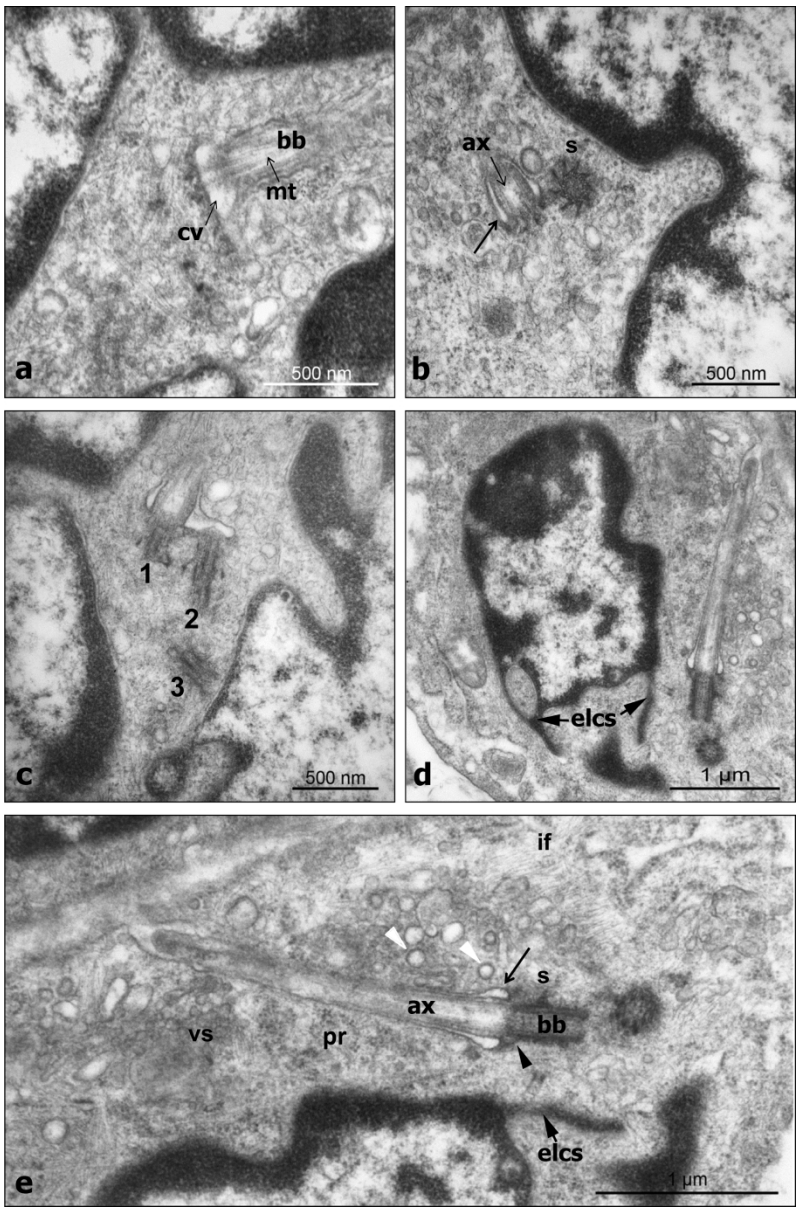

Fig.3. TEM examination. Primary cilia in stromal cells of GCTB. a) At the beginning of ciliogenesis, small vesicles derived from Golgi-apparatus fuse in a ciliary vesicle (cv) which localizes on top of the basal body (bb). Scale bar = 500nm b) Axoneme (ax) originates from basal body and is surrounded by a cell membrane invagination called ciliary pocket (cp). Daughter centriole shows pericentriolar satellites (s). Scale bar = 500nm c) Tumoral cells exceptionally showed centriole duplication, with two cilia emerging. Scale bar = 500nm d) SC shows envelope-limited chromatin sheet (elcs) and primary cilium. Scale bar = 1µm e) Primary cilium ultrastructural features. Scale bar = 1µm. mt: microtubule, if: intermediate filaments, pr: polyribosomes, vs: vesicles, sa: subdistal appendages, s: satellites, arrow: ciliary pocket, black arrowhead: transition fibers, white arrowhead: coated vesicles, bb: basal body, ax: axoneme.

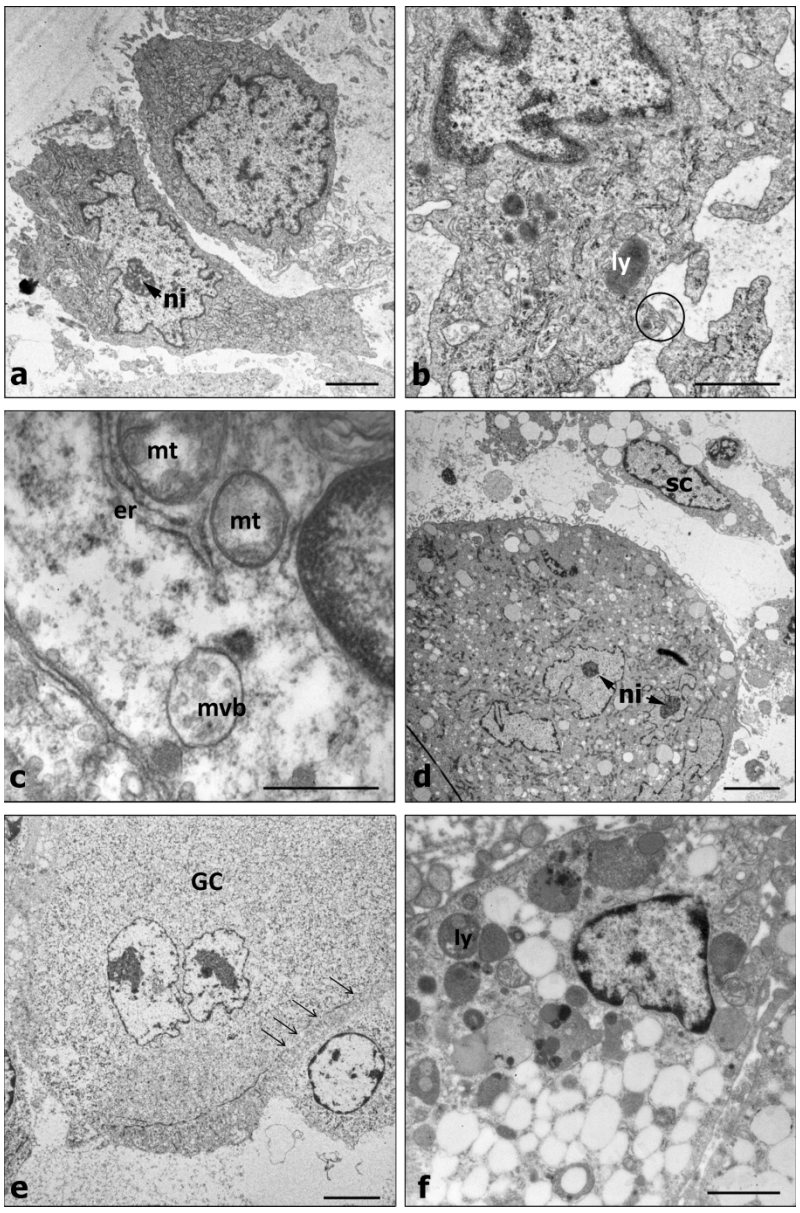

Fig.4. TEM examination. Ultrastructural features of reactive cells: histiocytic light cells and multinucleated giant cells. a) Histiocytic cells show less electrondense cytoplasm than SCs and prominent nucleoli (ni). Scale bar = 2μm b) Organelle distribution of histiocytic cells. Ly: lysosomes. Encircled: intercellular contact. Scale bar = 1μm c) Detailed area of histiocytic cells organelles showing mitochondria (mt) surrounded by endoplasmic reticula (er) near a multivesicular body (mvb). Scale bar = 500nm d) Giant Cells show multiple nuclei with prominent nucleoli (ni). Moreover, its cell membrane shows short prolongations. A stromal cell (SC) appears near the GC. Scale bar = 5μm e) A histiocytic cell seems to fuse with GC (arrows point cell membrane disappearance e). Scale bar = 5μm f) Foam cells sometimes show lysosomes (ly) containing inclusions of different source. Scale bar = 5μm

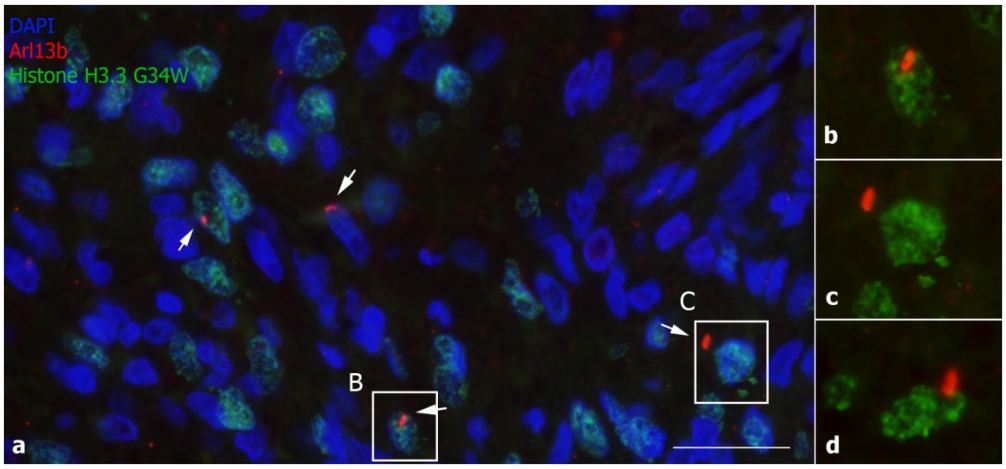

Fig.5. Stromal cells show primary cilia. a) Immunofluorescent co-localisation of Histone H3.3 G34W mutation in green and Arl13b (ciliary membrane) in red showed that some stromal cells present primary cilia. Scale bar = 20μm b-d) Magnification of cells showing Histone H3.3 G34W mutation and Arl13b co-localisation.

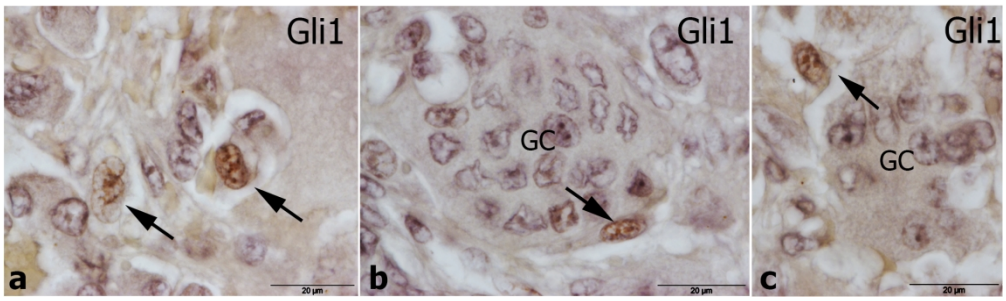

Fig. 6. Immunohistochemical study of Hh pathway activation. a-c) Nuclear labeling of Gli1 was present in some mononuclear cells, showing activation of Hh signaling pathway. GC: Giant Cell. Scale bar = 20μm

STROMAL CELLS OF GIANT CELL TUMOR OF BONE SHOW PRIMARY CILIA

PRIMARY CILIA IN GIANT CELL TUMOR OF BONE

Tomás Castiella MD, PhD[1(*)], Pablo Iruzubieta MD[2(*)], Eva Monleón PhD[2], Mª José Cardiel MD[1], Jesús Gómez-Vallejo MD[3], Marta Monzón PhD[2], Mª Concepción Junquera PhD[2]

1 Department of Pathology, Hospital ClínicoUniversitario Lozano Blesa

2 Department of Human Anatomy and Histology, Faculty of Medicine, University of Zaragoza

3 Department of Traumatology and Orthopaedic Surgery, Hospital ClínicoUniversitario Lozano Blesa

(*)TC and PI are first co-authors

Institute for Health Research Aragón (IIS), Domingo Miral s/n, 50009 Zaragoza, Spain

CorrespondingAuthor: *Pablo Iruzubieta, pablo.iruzubieta@hotmail.esPhone: 00 34 976 761674;*

ORCID:

Tomás Castiella: 0000-0001-7453-2470

Pablo Iruzubieta: 0000-0003-0331-6222

Eva Monleón: 0000-0002-7453-1766

Marta Monzón: 0000-0002-2787-9671

Concepción Junquera: 0000-0002-9951-107

ABSTRACT

Giant cell tumor of bone (GCTB) is a locally aggressive primary bone neoplasm composed by tumoral stromal cells and a reactive component that consists of monocytic/histiocytic cells that give rise by fusion to osteoclast-like multinucleated cells. Recently, specific histone 3.3 mutations have been demonstrated in stromal cells of GCTB. Many of the pathways related to bone proliferation and regulation depend on the primary cilium, a microtubule-based organelle which protrudes outside the cell and acts as a sensorial antenna. In the present work, we aimed to study the presence and role of primary cilia in GCTB.

Ultrastructural, immunohistochemical and immunofluorescence studies were performed in order to demonstrate, for the first time, that the primary cilium is located in spindle-shaped stromal cells of GCTB. Moreover, we showed Hhsignaling pathway activation in these cells. Hence, primary cilia may play a relevant role in GCTB tumorogenesis through Hh signaling activation in stromal cells.

Keywords: Giant cell tumor of bone, ultrastructural study, primary cilium, Hhsignaling pathway

Research highlights

- Transmission electron microscopy allows describing and differentiating cellular subpopulations in Giant Cell Tumor of Bone.
- The primary cilium is present in some tumoral Stromal Cells of Giant Cell Tumor of Bone.
- Hedgehog signalling is activated in these cells.

1. INTRODUCTION

According to the World Health Organisation (WHO) definition, giant cell tumor of bone (GCTB) is a locally aggressive primary bone neoplasm composed of proliferative mononuclear stromal cells (SCs) and numerous reactive macrophages and large osteoclast-like multinucleated giant cells (GCs) (Athanasou et al., 2013). GCTB usually appears in young adults' metaphysis-epiphysis of long tubular bones. Factors influencing the clinical course and biological aggressiveness of GCTB are unclear. Although malignant transformation in GCTB is uncommon, pulmonary metastasis have been described (Athanasou et al., 2013).

Two mixed mononuclear cell types are present in the GCTB: monocyte-macrophage CD14+/CD68+ cells and SCs (Wülling et al., 2003). Nowadays, it is accepted that SCs represent the proliferative tumoral component of the GCTB while reactive multinucleated GCs are originated from blood monocytes which are recruited into tumoral tissue (Kim et al., 2012; Wülling et al., 2003). Recently, Histone H3 G34W mutation has been proved as a useful diagnostic marker of SC in GCTB (Cleven et al., 2015).

Previous ultrastructural studies dealing with GCTB have been focused on characterization of mononuclear cells and their osteoblastic or osteoclastic differentiation (Anazawa et al., 2006; Aparisi et al., 1977; Garcia et al., 2013). Several reports have also described the ultrastructural similarities of GCTB giant cells with physiological osteoclasts and with multinucleated GC in lesions that mimic GCTB (Anazawa et al., 2006).

The primary cilium is a microtubular non-motile structure composed of a 9+0 axoneme originated from a modified centriole which projects to the extracellular medium (Malicki & Johnson, 2017). Its presence in skeletal cells was detected almost 50 years ago (Tonna & Lampen, 1972). However, the hypothesis that this organelle may play a role in regulating bone development and homeostasis was proposed in the beginning of the

twenty first century (Whitfield, 2003). There is increasing evidence that primary cilia-dependent signaling pathways, like Hedgehog (Hh) and Wnt, play a crucial role in regulating mammalian bone development and turnover (Day & Yang, 2008). Thus, Hh pathway activation is necessary for Runx2 expression, a transcription factor essential for correct osteoblast differentiation (Rutkovskiy et al., 2016).

Three Hh ligands have been described: Sonic (Shh), Indian (Ihh) and Desert (Dhh) (Ramsbottom & Pownall, 2016). Ihh has been mainly implicated in bone formation (Yang et al., 2015). When these ligands bind the transmembrane receptor Patched (located in the ciliary membrane) it is removed from primary cilia, allowing Smo entrance in ciliary axoneme. Then, Gli proteins are activated and translocated into the cellular nucleus, where they promote target gene transcription (including Runx2) (Chahal et al., 2018). Hh activation enhances expression of genes related to proliferation, angiogenesis or epithelial-mesenchymal transition (Chahal et al., 2018). Thus, excessive Hh signaling activation leads to tumor formation and maintenance of cancer stem cells (Chahal et al., 2018). Moreover, ciliary proteins, including Arl13b, have been shown to be essential in Hh signalling and in its oncogenic implications (Larkins et al., 2011; Bay et al., 2018).

Here, we show for the first time that SCs of GCTB present primary cilia, which may have important implications in these tumors through Hh signaling pathway activation.

2. METHODS

Six GCTB samples biopsied from patients were included in the present study. All samples were provided by the Hospital Clínico Lozano Blesa from Zaragoza. All the protocols developed were approved by the Human Research Ethics Committee of Aragon (CEICA) and were in accordance with Helsinki Declaration.

2.1. Electron Microscopy

A piece of every tumor consisting of 2.5x2.5mmwas immersed in 2.5% glutaraldehyde for fixation for 4-6h. The samples were washed in PB buffer solution, post-fixed with 2% osmium, rinsed, dehydrated in graded ethanol, stained with 2% uranyl-acetate, cleared in propylene oxide and embedded in araldite (Durcupan, Fluka). Serial semi-thin sections (1.5µm) were cut and lightly stained with 1% toluidine blue. Later, ultrathin (0.08µm) sections were cut with a diamond knife, collected on Formvar coated single-slot grids, counter-stained with 1% uranyl acetate and Reynold's lead citrate for 10minutes. They were examined by a JEOL-JEM-1010 transmission electron microscope (TEM). The images were captured with GatanBioscan Camera with pixel size 6.45µm x 6.45µm and spatial resolution of 1024,1024, 1, 1 (x, y, z, t) and automatic gain.

2.2. Immunohistochemistry

Immunohistochemical staining was performed on formalin-fixed paraffin-embedded sections 4-µm thick using EnVision® (Dako) method. The primary antibodies used in this study were: monoclonal rabbit anti-Histone H3.3 G34W (2.5 µg/mL, Quimigen S.L. 31-1145-00, Madrid, Spain), polyclonal rabbit anti-Gli1 (1:200, Abcam, ab49314, Cambridge, UK), polyclonal rabbit anti-Smo (1:1000, LS Bioscience, LS-B4911, Seattle, USA) and polyclonal goat anti-Patched (1:100, Santa Cruz, sc-6149, Dallas, USA). Antibodies were diluted with Dako diluents (S2022). The tissue sections were deparaffinize and hydrated using routine methods. Heat-induced antigen retrieval was performed. For Gli1 and Smo, buffer citrate ph6 (Dako S2031) was used and the samples were treated during 6 minutes in an 800-W microwave and at 360 W for 5 additional minutes. For H3.3 G34W and Patched staining, samples were treated with TBS (ph9) for 20 minutes at 96°C. Endogenous peroxidase was blocked using Dako S2001 peroxidase blocking reagent for 30 minutes and sections were washed in distilled water and PBS 3 min, twice.

Afterwards, sections were incubated with primary antibodies at 4°C overnight in a humidified chamber, washed in PBS three times and incubated with secondary antibody Rabbit-Mouse Labelled Polymer-DakoEnVision-HRP (K5007) or Polyclonal Rabbit Anti-Goat Immunoglobulins/HRP (1:200, Dako, P016002-2) for 1 hour. 3,3' diaminobenzidine was used as chromogene. The samples were washed twice in distilled water, contrasted with Mayer's hematoxylin for 7 min, washed in tap water for 15 min, dehydrated in a graded series of ethanol, cleared in xylene and coverslipped with Eukitt.

Negative controls where based on samples were no primary antibody was added. All antibodies were commercial and supposedly validated.

Whole samples were analysed and digital images from representative areas were captured by Olympus BX53 and Olympus UIS UPLFLN Series objectives. FN: 26.5. 20x AN 0.5 and 40x AN 0.75. Images were captured with Olympus DP72 Digital Camera. Pixel size 6.45µm x 6.45µm, total number of pixel 1.5 million. Exposition mode: SFL Auto and spatial resolution of 4140x3096x1x1 (x, y, z, t).

2.3. Double Immunofluorescence Microscopy

Formalin-fixed paraffin-embedded tissues were deparaffinize and hydrated and antigen retrieval was performed using TBS (pH9) at 96 °C for 20 min. Sections were incubated overnight at 4°C with the following antibodies: mouse-monoclonal anti-Acetylated tubulin (1:4000, Sigma Aldrich, T7451; St. Louis, MO, USA), mouse monoclonal anti-Arl13b (1:50, Proteintech, 66739-1-Ig, Manchester, UK) and rabbit-monoclonal anti-Histone H3.3 G34W (2.5 µg/mL, Quimigen S.L., 31-1145-00, Madrid, Spain). They were washed in PBS for 5 minutes (three times) and incubated with the respective secondary antibodies: anti-Mouse AlexaFluor594 (1:1000, ThermoFisher R37115; Waltham, MA, USA) and anti-Rabbit AlexaFluor488 (1:1000, ThermoFisher A-21206; Waltham, MA, USA) for 1 hour at RT. Incubations were performed in a dark humidified

chamber. After washing in PBS, DAPI (1 µg/mL, Sigma-Aldrich) was added for 1 minute for nuclei counterstaining. Sections were washed in PBS and cover with DAKO Fluorescence mounting medium.

Whole samples were analysed and digital images from representative areas were captured by Olympus BX53 and Olympus UIS UPLFLN Series objectives. FN: 26.5. 20x AN 0.5 and 40x AN 0.75. Images were captured with Olympus DP72 Digital Camera. Pixel size 6.45µm x 6.45µm, total number of pixel 1.5 million. Exposition mode: SFL Auto and spatial resolution of 4140x3096x1x1 (x, y, z, t).

All antibodies were commercial and supposedly validated.

Images were analysed using the following filters: U-MNUA2 for DAPI, U-MWIABA2 for Alexa Fluor 488 and U-MWIG2 for Alexa Fluor 594 in a Olympus BX53 microscope and Olympus UIS UPLFLN Series objectives. FN: 26.5. 20x AN 0.5 and 40x AN 0.75. Images were captured with Olympus DP72 Digital Camera. Pixel size 6.45µm x 6.45µm, total number of pixel 1.5 million. Exposition mode: Auto and spatial resolution of 4080x3072x1x1 (x, y, z, t).

Images were analysed with DP Controller Software. Every fluorescent channel was individually photographed and channels were merged using FIJI Image_J software, where contrast and brightness were adjusted (Schindelin et al., 2012).

Statistical analyses were performed counting ciliated cells per High Power Field (HPF = x400) and using a non parametric test (Mann-Whitney U). Hence, representative areas were analysed (total of 18 images). In each HPF, between 70 and 100 mononuclear cells were present while the number of giant cells ranges from 0 to 7.

3. RESULTS

3.1. Preliminary histological study.

Hematoxylin-Eosin (HE) and general immunohistochemistry confirmed the diagnosis of GCTB (Fig.1). Thus, HE revealed the presence of multinuclear giant cells (GCs)

scattered among mononuclear cells (Fig.1a). CD68 antibody marked mononuclear histiocytic cells and multinucleated GCs (Fig.1b) while Histone H3.3 mutation G34W antibody labelled tumoral stromal cells (SCs) (Fig.1c). Ki67 was exclusively expressed by mononuclear cells (Fig.1d).

3.2. Ultrastructure of GCTB

Electron microscopy examination evidenced two well-defined groups: mononuclear and multinucleated giant cells. In turn, mononuclear cells included two distinguishable phenotypes based on cytoplasm electrondensity and nuclear chromatin condensation. Thus, histiocytic cells showed lesser electrondensity and homogenous chromatin, while SCs cytoplasm were more electrondense and their nuclei showed condensed chromatin constituting marginal clusters in contact with nuclear envelope (Fig.2a).

SCs morphology varied from fusiform spindle to oval shapes. They showed fine membrane prolongations contacting neighbour cells (Fig.2b). They presented cytoplasmic electron-light no-membranous inclusions conferring a characteristic vacuolated appearance (Fig.2b). Some mitochondria, scarce granular endoplasmic reticulum and abundant free ribosomes were observed. Centrioles, located near nuclei, showed subdistal appendages and they were related to intermediate filaments and numerous Golgi-derived vesicles (Fig.2c-d). All these findings are suggestive of centriolar activation.

Primary cilia were specifically observed in SCs (Fig.2e-f). Primary ciliogenesisis sequentially ordered in Figure 3. Firstly, the ciliary vesicle (constituted by fusion of Golgi-derived vesicles) localizes on the distal pole of the mother centriole, which forms cilia basal body (Fig.3a). Then, the 9+0 axoneme grows from the basal body (Fig. 3b). Occasionally, abnormal duplication of centrioles was evidenced by detection of three centrioles, two of them originating cilia (Fig.3c). Figures 3d and 3e show a primary cilium in its maximum length and its ultrastructural features are also showed. Basal

body presented subdistal appendages and was anchored to cell membrane by transition fibers. The axoneme was originated from the basal body and it was located in a cell membrane invagination called ciliary pocket, where coated vesicles are concentrated as a sign of important molecular exchange (Fig.3e). In some ciliated cells, nuclei showed characteristic nuclear envelope prolongations (Fig. 3d-e). These nuclear structures have been previously called envelope-limited chromatin sheets (ELCS). It is relevant to emphasize that primary cilia in these cells are originated from no-displaced centrioles and, therefore, goes through the cytoplasm towards the extracellular medium.

The mononuclear histiocytic cells showed a less electrondense cytoplasm (Fig.4a), with abundant mitochondria, granular endoplasmic reticulum and prominent Golgi apparatus. Although their nuclei showed a diverse morphology, peripheral nucleoli were always found. According to their histiocytic nature, they presented many lysosomes and fine phagocytic prolongations (Fig.4b). These cells contact each other through cytoplasmic prolongations (Fig.4b). A reduced number of these histiocytic cells showed scarce organelles, abundant ribosomes and multivesicular bodies, features suggestive of undifferentiated phenotype (Fig. 4c).

Multinucleated GCs included 10 to 30 nuclei. They showed oval or irregular morphology and an electron light appearance. They presented a fine marginal chromatin contacting nuclear membrane and prominent nucleoli (Fig.4d). Their cytoplasm presented a homogenous distribution of organelles, abundant mitochondria and lipid inclusions (Fig. 4d). Surrounding multinucleated GCs, both, mononuclear histiocytic and stromal cells were located. Although defining dynamic processes from TEM is always difficult, we could observe light undifferentiated histiocytic cells merging with GCs and syncytial membrane disappearance, suggestive of cellular fusion (Fig.4e).

Some reactive foam cells plenty of electron lucent vacuoles were also found in these tumors. They were probably involved in phagocytic processes as they showed lysosomes with different content (Fig.4f). Few disperse lymphocytes and granulocytes were also observed, the latter being involved in macropinocytosis processes.

3.3. Primary cilia and Hedgehog signaling presence in GCTB

Immunofluorescent co-localisation of Histone H3.3 mutation G34W (specific for SCs of GCTB) and Acetylated-tubulin (marker for cilia axoneme) and Arl13b (marker for ciliary membrane) showed that stromal cells presented primary cilia (Fig. 5, Suppl. Fig. 1). Primary cilia were usually located near nuclei, in agreement with electron microscopy findings. A quantitative analyses showed that around 7 mononuclear cells per High Power Field (x400) were ciliated, which supposed around 10% of mononuclear cells, while no multinucleated giant cell presented cilia (Suppl. Fig.2).

Furthermore, we studied the implications of primary cilia in GCTB analysing the activation of Hedgehog (Hh) signaling pathway, a well-known cilia-dependent pathway related to tumorogenesis and bone regulation. Immunohistochemical experiments for Hh pathway protein Patched, Smo and Gli1 were performed (Suppl. Fig. 3, Fig. 6). Patched (Suppl. Fig. 3a) and Smo (Suppl. Fig. 3b) staining were located in paranuclear regions while Gli1 labelled subtly but clearly cells nuclei (Fig. 6a-c). Nuclear staining of Gli1 is an indisputable sign of Hh signaling activation.

Thus, these results suggest that Hh signaling pathway is present and activated in SCs of GCTB.

4. DISCUSSION

The nature and cellular components of GCTB have been the subject of multiple previous studies, most of which have wrongly identified all mononuclear cells as

stromal cells based on conventional microscopy morphology. However, histochemical and electron microscopy techniques shed light on cells identification (Aparisi et al., 1977; Hanaoka et al., 1970). In this study we have accurately defined ultrastructural features of the two different mononuclear cell populationsnidentified by cytoplasm electrondensity and nuclear chromatin condensation. Cells showing lesser electrodensity and homogenous chromatin are called histiocytic cells here. The round histiocytic cells previously described by other authors may correspond to activated histiocytes with phagocytic capacity (Aparisi et al., 1977; Hanaoka et al., 1970). Intermediate phenotypes are compatible with resting, activated or prior to giant cell formation stages.

The second mononuclear cell type, stromal cells (SCs), show more electrondense cytoplasm and nuclei with condensed chromatin forming marginal clusters in contact with nuclear envelope corresponding to stromal cells type 1 of Aparisi (Aparisi et al., 1977). However, phenotypic variability appears. Probably, those presenting features suggestive of undifferentiation may suppose cancer stem cells. SCs have been defined as immature fibroblasts or primitive osteoblasts. Their close histogenetic relation with osteoblasts is based on focal deposition of osteoid seen in one third of GCTB (Spjut et al., 1983). Additionally, bone tissue is not only produced by reactive osteoblasts but also by SCs (Goldring et al., 1987). According with the results provided here, SCs are clearly defined as mesenchymal cells presenting special and exclusive ultrastructural features such as presence of large electron-light vacuoles, peculiar density of cytoplasm and activation of centrioles. The most novel finding provided in the present study is the presence of primary cilia in these cells.

Primary cilia in osteoblasts and osteocytes contributes to bone formation and homeostasis (Mitchison & Valente, 2017). Furthermore, the participation of primary cilia in different types of cancer of epithelial and mesenchymal line has been demonstrated.

Nevertheless, the prevalence of cilia on human tumors remains unclear, and their role in cancer is just beginning to be explored (Eguether & Hahne, 2018; Fabbri et al., 2019). In human osteosarcoma MG63 cell line the number of ciliated cell is significantly higher than expected (Kowal & Falk, 2015).

The cilia-dependant Hh signaling pathway plays a key role in both bone physiology and pathology. Thus, it is essential for temporal and spatial regulation of bone remodelling (Rodda, 2006; Yang et al., 2015). Moreover, Hh signaling pathway (especially through the Ihh ligand) stimulates intramembranous and endochondral ossification, bone turnover and remodeling of fractures sites (Yang et al., 2015).

The deregulation of Hh signaling pathway has been linked to some skeletal development diseases (Rodda, 2006; Yang et al., 2015) and tumors (Scales & de Sauvage, 2009). Furthermore, Hh signaling pathway in osteosarcoma was related to radioresistance and invasiveness (Qu et al., 2018). Interestingly, the ciliary membrane protein Arl13b plays an essential role in tumoral Hh signaling through primary cilia (Bay et al., 2018).

Here, we show Hh pathway activation in some SCs. These results are in accordance with Horvai et al. (Horvai et al., 2012) where 10% of mononucleated cells expressed Ihh (we found a similar proportion of ciliated cells, as it is described above). Besides, Horvai et al. also showed that GCTB stromal cells expressed Runx2 (Horvai et al., 2012) a well-known downstream target of Hh signaling pathway (Rutkovskiy et al., 2016).

The observation of primary cilia and Hh pathway activation in SCs suggests their role in cellular signaling and tumorogenesis. Moreover, some ciliated SCs showed envelope-limited chromatin sheets (ELCS), a structure described in cancer and stem cells (Olins & Olins, 2009; Cebrián-Silla et al., 2017). These findings suggest that primary cilia may play an important role in quiescent cancer stem cells of GCTB. This feature would

explain why only a specific population of stromal cells show primary cilia and Hh activation and they are not constitutively present in every stromal cell. Moreover, the dynamic nature of cilia assembly and Hh signaling must be taken into account while the techniques performed in this paper are mainly static.

In conclusion, our study reveals that SCs of GCTB present primary cilia. Moreover, we proved that Hh signaling pathway is activated in these cells, showing that primary cilia may play an important role in GCTB tumorogenesis and could be used as a potential therapeutic target.

5. DECLARATIONS

Funding. No funding was specifically received for the experiments showed in this paper.

Competing interests. The authors declare that they have no conflict of interest.

Ethics approval and consent declarations. All protocols and consents developed were approved by the Human Research Ethics Committee “Comité Ético de Investigación Clínica de Aragón”.

Authors contribution. TC conceived the study, performed ultrastructural experiments and contributed to write the manuscript, PI performed immunohistochemical and immunofluorescence studies and contributed to write the manuscript, EM performed immunohistochemical experiments. MJC and JGV provided the samples. MM contributed to write the manuscript. CJ conceived and supervised the study, performed ultrastructural experiments, analysed the results and contributed to write the manuscript.

Acknowledgements: Authors would like to acknowledge the use of *Servicio General de Apoyo a la Investigación*- SAI, *Universidad de Zaragoza*.

6. REFERENCES

Anazawa, U., Hanaoka, H., Shiraishi, T., Morioka, H., Morii, T., & Toyama, Y. (2006). Similarities between giant cell tumor of bone, giant cell tumor of tendon sheath, and pigmented villonodular synovitis concerning ultrastructural cytochemical features of multinucleated giant cells and mononuclear stromal cells. *Ultrastructural Pathology*, *30*(3), 151–158. https://doi.org/10.1080/01913120600689707

Aparisi, T., Arborgh, B., & Ericsson, J. L. (1977). Giant cell tumor of bone: detailed fine structural analysis of different cell components. *Virchows Archiv. A, Pathological Anatomy and Histology*, *376*(4), 273–298. http://www.ncbi.nlm.nih.gov/pubmed/145722

Athanasou, N., Bansal, M., Forsyth, R., Reid, R., & Z, S. (2013). Giant Cell Tumour of Bone. In C. Fletcher, J. Bridge, P. Hogendoorn, & F. Mertens (Eds.), *WHO Classification of Tumours of Soft Tissue and Bone* (pp. 321–324). IARC.

Bay, S. N., Long, A. B., & Caspary, T. (2018). Disruption of the ciliary GTPase Arl13b suppresses Sonic hedgehog overactivation and inhibits medulloblastoma formation. *Proceedings of the National Academy of Sciences of the United States of America*, *115*(7), 1570–1575. https://doi.org/10.1073/pnas.1706977115

Cebrián-Silla, A., Alfaro-Cervelló, C., Herranz-Pérez, V., Kaneko, N., Park, D. H., Sawamoto, K., Alvarez-Buylla, A., Lim, D. A., & García-Verdugo, J. M. (2017). Unique Organization of the Nuclear Envelope in the Post-natal Quiescent Neural Stem Cells. *Stem Cell Reports*, *9*(1), 203–216. https://doi.org/10.1016/j.stemcr.2017.05.024

Chahal, K. K., Parle, M., & Abagyan, R. (2018). Hedgehog pathway and smoothened inhibitors in cancer therapies. *Anti-Cancer Drugs*, *29*(5), 387–401. https://doi.org/10.1097/CAD.0000000000000609

Cleven, A. H. G., Höcker, S., Briaire-De Bruijn, I., Szuhai, K., Cleton-Jansen, A. M., & Bovée, J. V. M. G. (2015). Mutation analysis of H3F3A and H3F3B as a diagnostic tool for giant cell tumor of bone and chondroblastoma. *American Journal of Surgical Pathology*, *39*(11), 1576–1583. https://doi.org/10.1097/PAS.0000000000000512

Day, T. F., & Yang, Y. (2008). Wnt and hedgehog signaling pathways in bone development. *Journal of Bone and Joint Surgery - Series A*, *90*(SUPPL. 1), 19–24. https://doi.org/10.2106/JBJS.G.01174

Eguether, T., & Hahne, M. (2018). Mixed signals from the cell's antennae: primary cilia in cancer. *EMBO Reports*, *19*(11), e46589. https://doi.org/10.15252/embr.201846589

Fabbri, L., Bost, F., & Mazure, N. (2019). Primary Cilium in Cancer Hallmarks. *International Journal of Molecular Sciences*, *20*(6), 1336. https://doi.org/10.3390/ijms20061336

Garcia, R. A., Platica, C. D., Alba Greco, M., & Steiner, G. C. (2013). Myofibroblastic differentiation of stromal cells in giant cell tumor of bone: An immunohistochemical and ultrastructural study. *Ultrastructural Pathology*, *37*(3), 183–190. https://doi.org/10.3109/01913123.2012.756092

Goldring, S. R., Roelke, M. S., Petrison, K. K., & Bhan, A. K. (1987). Human giant cell tumors of bone. Identification and characterization of cell types. *Journal of Clinical Investigation*, *79*(2), 483–491. https://doi.org/10.1172/JCI112838

Hanaoka, H., Friedman, B., & Mack, R. P. (1970). Ultrastructure and histogenesis of giant-cell tumor of bone. *Cancer*, *25*(6), 1408–1423. https://doi.org/10.1002/1097-0142(197006)25:6<1408::aid-cncr2820250622>3.0.co;2-#

Horvai, A. E., Roy, R., Borys, D., & O'Donnell, R. J. (2012). Regulators of skeletal development: A cluster analysis of 206 bone tumors reveals diagnostically useful markers. *Modern Pathology*, *25*(11), 1452–1461. https://doi.org/10.1038/modpathol.2012.110

Kim, Y., Nizami, S., Goto, H., & Lee, F. Y. (2012). Modern interpretation of giant cell tumor of bone: Predominantly osteoclastogenic stromal tumor. *Clinics in Orthopedic Surgery*, *4*(2), 107–116. https://doi.org/10.4055/cios.2012.4.2.107

Kowal, T. J., & Falk, M. M. (2015). Primary cilia found on HeLa and other cancer cells. *Cell Biology International*, *39*(11), 1341–1347. https://doi.org/10.1002/cbin.10500

Larkins, C. E., Gonzalez Aviles, G. D., East, M. P., Kahn, R. A., & Caspary, T. (2011). Arl13b regulates ciliogenesis and the dynamic localization of Shh signaling proteins. *Molecular Biology of the Cell*, *22*(23), 4694–4703. https://doi.org/10.1091/mbc.E10-12-0994

Malicki, J. J., & Johnson, C. A. (2017). The Cilium: Cellular Antenna and Central Processing Unit. *Trends in Cell Biology*, *27*(2), 126–140. https://doi.org/10.1016/j.tcb.2016.08.002

Mitchison, H. M., & Valente, E. M. (2017). Motile and non-motile cilia in human pathology: from function to phenotypes. *Journal of Pathology*, *241*(2), 294–309. https://doi.org/10.1002/path.4843

Olins, D. E., & Olins, A. L. (2009). Nuclear envelope-limited chromatin sheets (ELCS) and heterochromatin higher order structure. *Chromosoma*, *118*(5), 537–548. https://doi.org/10.1007/s00412-009-0219-3

Qu, W., Li, D., Wang, Y., Wu, Q., & Hao, D. (2018). Activation of Sonic Hedgehog Signaling Is Associated with Human Osteosarcoma Cells Radioresistance Characterized by Increased Proliferation, Migration, and Invasion. *Medical Science Monitor*, *24*, 3764–3771. https://doi.org/10.12659/MSM.908278

Ramsbottom, S., & Pownall, M. (2016). Regulation of Hedgehog Signalling Inside and Outside the Cell. *Journal of Developmental Biology*, *4*(3), 23. https://doi.org/10.3390/jdb4030023

Rodda, S. J. (2006). Distinct roles for Hedgehog and canonical Wnt signaling in specification, differentiation and maintenance of osteoblast progenitors. *Development*, *133*(16), 3231–3244. https://doi.org/10.1242/dev.02480

Rutkovskiy, A., Stensløkken, K.-O., & Vaage, I. J. (2016). Osteoblast Differentiation at a Glance. *Medical Science Monitor Basic Research*, *22*, 95–106. https://doi.org/10.12659/MSMBR.901142

Scales, S. J., & de Sauvage, F. J. (2009). Mechanisms of Hedgehog pathway activation in cancer and implications for therapy. *Trends in Pharmacological Sciences*, *30*(6), 303–312. https://doi.org/10.1016/j.tips.2009.03.007

Schindelin, J., Arganda-Carreras, I., Frise, E., Kaynig, V., Longair, M., Pietzsch, T., Preibisch, S., Rueden, C., Saalfeld, S., Schmid, B., Tinevez, J., White, D. J., Hartenstein, V., Eliceiri, K., Tomancak, P., & Cardona, A. (2012). Fiji: an open-source platform for biological-image analysis. *Nature Methods*, *9*(7), 676–682. https://doi.org/10.1038/nmeth.2019

Spjut, H., Dorfman, H. D., Robert E., F., & Lauren V., A. (1983). *Atlas of tumor pathology. Tumors of bone and cartilage.* (1983), Armed Forces Institute of Pathology.

Tonna, E. A., & Lampen, N. M. (1972). Electron microscopy of aging skeletal cells. I. Centrioles and solitary cilia. *Journal of Gerontology*, *27*(3), 316–324. http://www.ncbi.nlm.nih.gov/pubmed/5046597

Whitfield, J. F. (2003). Primary cilium - Is it an osteocyte's strain-sensing flowmeter? *Journal of Cellular Biochemistry*, *89*(2), 233–237. https://doi.org/10.1002/jcb.10509

Wülling, M., Delling, G., & Kaiser, E. (2003). The Origin of the Neoplastic Stromal Cell in Giant Cell Tumor of Bone. *Human Pathology*, *34*(10), 983–993. https://doi.org/10.1053/S0046-8177(03)00413-1

Yang, J., Andre, P., Ye, L., & Yang, Y. Z. (2015). The Hedgehog signalling pathway in bone formation. *International Journal of Oral Science*, *7*(2), 73–79. https://doi.org/10.1038/ijos.2015.14

FIGURE LEGENDS

Fig. 1. Histological diagnosis and preliminary study of GCTB. a) Hematoxylin-Eosin staining shows two cellular types in GCTB: mononuclear and multinuclear giant cells (GC). Some of the mononuclear cells showed a characteristic paranuclear vacuole (arrow). Scale bar = 50μm b) CD68 is a specific marker for monocyte-macrophage lineage. Thus, histiocytic mononuclear cells and giant cells (GC) expressed CD68. Scale bar = 50μm c) Histone H3.3 G34W mutation is a specific marker of the stromal neoplastic cells of GCTB. According to this, only mononuclear cells were stained, some of them expressing paranuclear vacuoles (arrow).Scale bar = 50μm d) Immunolabeling for Ki67, marker of cell cycle activation and proliferation, stained uniquely mononuclear cells. Scale bar = 100μm

Fig.2. TEM examination. Ultrastructural features of mononuclear cells of GCTB. a) Histiocytic (* light) and stromal (dark) cells are the main mononuclear components of GCTB. Scale bar = 5μm b) Stromal cells (SCs) show large paranuclear vacuoles (v). Scale bar = 2μm c-d) Centriole activation at different stages. Note the numerous small vesicles (vs), subdistal appendages (s) and intermediate filaments (if) in relation with centrioles; features related to centriolar activation. Scale bar = 500nm e) Primary cilia in a SC. Scale bar = 2μm f) Magnification of squared area in e. Scale bar = 500nm. ax: axoneme, bb: basal body, v: vacuoles, vs: vesicles, if: intermediate filaments, mt: microtubule, s: subdistal appendages, g: Golgi

Fig.3. TEM examination. Primary cilia in stromal cells of GCTB. a) At the beginning of ciliogenesis, small vesicles derived from Golgi-apparatus fuse in a ciliary vesicle (cv) which localizes on top of the basal body (bb). Scale bar = 500nm b) Axoneme (ax) originates from basal body and is surrounded by a cell membrane invagination called

ciliary pocket (cp). Daughter centriole shows pericentriolar satellites (s). Scale bar = 500nm c) Tumoral cells exceptionally showed centriole duplication, with two cilia emerging. Scale bar = 500nm d) SC shows envelope-limited chromatin sheet (elcs) and primary cilium. Scale bar = 1µm e) Primary cilium ultrastructural features. Scale bar = 1µm. mt: microtubule, if: intermediate filaments, pr: polyribosomes, vs: vesicles, sa: subdistal appendages, s: satellites, arrow: ciliary pocket, black arrowhead: transition fibers, white arrowhead: coated vesicles, bb: basal body, ax: axoneme.

Fig.4. TEM examination. Ultrastructural features of reactive cells: histiocytic light cells and multinucleated giant cells. a) Histiocytic cells show less electrondense cytoplasm than SCs and prominent nucleoli (ni). Scale bar = 2µm b) Organelle distribution of histiocytic cells. Ly: lysosomes. Encircled: intercellular contact. Scale bar = 1µm c) Detailed area of histiocytic cells organelles showing mitochondria (mt) surrounded by endoplasmic reticula (er) near a multivesicular body (mvb). Scale bar = 500nm d) Giant Cells show multiple nuclei with prominent nucleoli (ni). Moreover, its cell membrane shows short prolongations. A stromal cell (SC) appears near the GC. Scale bar = 5µm e) A histiocytic cell seems to fuse with GC (arrows point cell membrane disappearance e). Scale bar = 5µm f) Foam cells sometimes show lysosomes (ly) containing inclusions of different source. Scale bar = 5µm

Fig.5. Stromal cells show primary cilia. a) Immunofluorescent co-localisation of Histone H3.3 G34W mutation in green and Arl13b (ciliary membrane) in red showed that some stromal cells present primary cilia. Scale bar = 20µm b-d) Magnification of cells showing Histone H3.3 G34W mutation and Arl13b co-localisation.

Fig. 6. Immunohistochemical study of Hh pathway activation. ~~a) Some mononuclear cells showed paranuclear staining forPatchedb) Similarly, only mononuclear cells showed paranuclear expression of Smo~~ a-c) Nuclear labeling of Gli1

was present in some mononuclear cells, showing activation of Hh signaling pathway. GC: Giant Cell. Scale bar = 20µm

Supplementary Fig. 1. Immunofluorescence study of primary cilia in SCs GCTB. Co-localisation of Acetylated tubulin (red) and H3.3 G34W (green) give supporting evidence of cilia in SCs of GCTB. Scale bar = 50µm

Supplementary Fig. 2. Quantitative analysis of primary cilia presence in GCTB cells. Number of cells showing primary cilia per High-Power Field (HPF: x400). 18 representative images were analysed in total. In each HPF, between 70 and 100 mononuclear cells were present while the number of giant cells ranges from 0 to 7. No multinucleated giant cells showed primary cilia, while around 7 to 8 mononucleated cells (mean of 7,53) per HPF were ciliated (approximately 10% of total mononucleated cells). Results are expressed as mean ± SEM. Mann-Whitney U Test showed a statistical significance ($p<0,00001$).

Supplementary Fig. 3. Smo and Patched staining in GCTB. a) Some mononuclear cells showed paranuclear staining for Patched. Scale bar = 20µm b) Similarly, only mononuclear cells showed paranuclear expression of Smo. Scale bar = 20µm.